PHYSICAL REVIEW B VOLUME 11, NUMBER 2 15 JANUARY 1975

Comparison of experiment and theory for tunneling in In-Ge:P Schottky-barrier junctions*

J. E. Christopher, H. M. Darley, G. W. Lehman, and S. N. Tripathi

Department of Physics and Astronomy, University of Kentucky, Lexington, Kentucky 40506

(Received 23 September 1974)

Schottky-barrier tunnel junctions were prepared by evaporating indium on (100), vacuum-cleaved faces of phosphorus-doped germanium crystals. Measurements of dV/dI versus bias voltage were made at liquid-helium temperatures and compared to theoretical predictions for one-electron tunneling through a Schottky barrier. The theory includes the effects of the germanium ellipsoidal energy surfaces and upper-conduction-band minimum (Γ_2'). All parameters used in the theory were determined by independent measurements. Order-of-magnitude agreement between theory and experiment was found which due to the large uncertainty in the parameters used in the theory is all that can be expected. The possibility of distinguishing differences between junctions made on germanium doped with antimony, arsenic, and phosphorus are discussed. Also included is a comparison of experiment and theory for phonon-assisted tunneling.

I. INTRODUCTION

A detailed comparison of experiment and theory has been reported[1,2] for metal–Ge: As and metal–Ge:Sb tunnel junctions. The measured resistance was compared with the one-electron theory of Conley, Duke, Mahan, and Tiemann[3] (CDMT), with all parameters determined by measurements other than tunneling. Agreement with theory was found for the shape and magnitude of the resistance for the antimony-doped junctions. Shape and order of magnitude agreement was found for arsenic-doped junctions. The question naturally arises: What results would a third dopant, phosphorus, give? This is particularly interesting in light of the work of Combescot and Schreder,[4] who have made theoretical estimates of impurity-assisted tunneling for metal–Ge (n type) junctions and predict different magnitudes for the different types of dopant. In this paper we present a detailed comparison of experiment and one-electron theory for phosphorus-doped germanium junctions. As in the work for other dopants,[1,2] all parameters in the theory were determined by independent measurements.

The theory to which the comparisons are made is basically the same as CDMT, however, some refinements are included. CDMT used the wave-function-matching procedure to evaluate the transmission probability, and in evaluating this used asymptotic approximations for the parabolic cylinder functions. In this work this approximation is avoided. The final expression to be evaluated in CDMT involved evaluating a double quadrature. This has been reduced to a single quadrature, making computer evaluation easier. The effects of the ellipsoidal energy surfaces were discussed by CDMT, but the calculations and results were not published. In this work calculations using the matching procedure and including this band structure are shown. This refinement was also treated in detail by Stratton and Padovani[5] using the WKB technique. Another refinement included in the theory presented here is a treatment of the tunneling into the Γ_2' conduction band. This edge is at an energy of 0.154 eV above the bottom of the conduction bands at the L_1 points.[6] When bias is applied such that direct tunneling from the metal to this band is possible, increased tunneling is predicted and is observed as a decrease in the resistance. Comparisons of theory and experiment for this resistance decrease are presented.

In addition to the detailed treatment of the direct tunneling, a comparison of the measured conductance changes due to phonon-assisted tunneling is compared to theoretical[1,7] predictions.

II. EXPERIMENTAL PROCEDURE

The samples were cut from a degenerately doped Ge:P single crystal. The sample size was $12\times4\times2$ mm. The long axis was the [100], so that the cleaved face was a (100) plane.

Ohmic contacts to one end of the sample were made by gold-bonding techniques. These contacts were checked for linearity and low impedance.

The samples were vacuum cleaved in an evaporating stream of In in a system based on the methods of Wolf and Compton.[8] As the sample was cleaved, a spring-loaded mask snapped in front of the cleaved face. This created a pattern of 0.2-mm dots on the cleaved surface. One dot was selected by means of the photoresist techniques of Cullen, Wolf, and Compton.[9] Contact to the In was then made by silver paint. To reduce unwanted capacitance between the silver paint and the semiconductor bulk, the photoresist around the dot was thickened by painting on additional photoresist.

The incremental resistance dV/dI was measured using standard techniques,[10,2] digitally recorded, and stored on magnetic tape for computer analysis. For example, the computer was used to determine dI/dV and d^2I/dV^2. The error in most measure-

ments of dV/dI is estimated to be 1%. For comparison to theory, the data are presented in terms of AdV/dI, where A is the junction area. The error in the area determination is estimated to be 20%. All samples were measured at 4.2 °K. Several samples were also measured at about 1.3 °K to sharpen the phonon steps. On these samples, a strong superconducting peak was observed, proving that the current mechanism was tunneling.

The barrier heights were determined by measuring the junction capacitance versus bias voltage at 77 °K. This procedure is outlined in Ref. 2. A Wayne Kerr B602 Universal rf Bridge was used. A capacitor was used in series with the sample to balance out the inductance of the leads of the jig. The frequency was adjusted until the capacitive reactance balanced the inductive reactance. This occured at about 6 MHz. The error in the value of the barrier height determined in this manner is estimated to be 5%. All of the measured values fell within 0.64 ± 0.03 eV, which compares well with other measurements.

Hall coefficients were measured to determine the carrier concentrations. The Hall-effect samples were cut from the halves of the dV/dI samples that were cleaved off. A 4×2×1.2 mm sample was cut as close to the cleaved face as possible. Measurements were performed at 77 °K. On several samples room-temperature measurements were taken and gave identical results within experimental error (5%). At the same time, room-temperature bulk-resistivity measurements were made on all samples. The carrier concentrations determined from the resistivity and published[11] resistivity-concentration plots were lower than those determined from the Hall coefficient, but within experimental error (± 5% on both resistivity and Hall coefficient). In all calculations, the values obtained from Hall coefficients were used.

III. THEORY

Numerous calculations of the tunneling current appropriate to the tunnel junctions discussed in this paper have been made using a one-electron formalism developed by Fredkin and Wannier[12] for p-n junctions. CDMT extended this analysis to the case of one-electron tunneling in n-Ge Schottky barriers. In their original paper, CDMT used an asymptotic expansion for the parabolic cylindrical functions in order to facilitate the calculation of the transmission coefficient. This approximation has been the subject of some criticism or, perhaps, concern. A further numerical concern occurs owing to the double quadrature in evaluating the CDMT current expression. In the case of ellipsoidal energy surfaces more appropriate to Ge, one is faced with a triple quadrature.

The theoretical contributions to this paper are two-fold. Our starting point is the Fredkin-Wannier current-density expression used by CDMT. Firstly, ellipsoidal energy surfaces are used, and an efficient numerical formalism is evolved for calculating the appropriate transmission coefficient for an arbitrarily specified barrier potential. Secondly, we use some analytic tricks to reduce the triple quadrature to a single-energy quadrature for an arbitrary barrier potential at zero temperature. The mathematical details are cumbersome and are relegated to two appendixes to this paper.

Our initial analysis follows CDMT. The current density flowing through a tunnel junction is

$$j = \frac{2e}{(2\pi)^3} \int_{k_{lz}>0} d^3k_l \, |T_{l\to r}|^2 v_{rz} [F(E_l) - F(E_l - V_a)], \qquad (1)$$

where d^3k_l is the volume element, $k_l^2 dk_l \sin\theta \, d\theta \, d\phi$ in wave-vector space. Here, k_l is the magnitude of the wave vector in the metal contact on the left. (The subscript l refers to left and is not to be confused with longitudinal-mass subscript used later.) The subscript z refers to an axis normal to surface of the crystal. This is the current-carrying axis, and v_{rz} is the electron velocity along this axis. For ellipsoidal energy surfaces, Stratton and Padavoni[5] show by a simple analysis that the effective mass m_r used by CDMT should be replaced by

$$m_r = [(\cos^2\Theta)/m_{\rm long} + (\sin^2\Theta)/m_{\rm tr}]^{-1}, \qquad (2)$$

where $m_{\rm tr}$, $m_{\rm long}$, and Θ are the transverse mass, longitudinal mass, and angle between the z axis and the longitudinal axis of the energy ellipsoid. With these observations, one can easily see that the CDMT formalism is trivially modified to handle ellipsoidal surfaces.

The energy E (or E_l) is measured from the top of the Fermi level ζ_l in the metal contact on the left. For a free-electron gas representing the metal, one has

$$E + \zeta_l = (\hbar^2/2m_l)k_l^2, \qquad (3)$$

where m_l and $\hbar$ are the effective mass for the metal contact and Planck's constant divided by 2π, respectively. In Eq. (1), $F(E_l)$ is the Fermi function.

Similarly, let k_{lz} be the component of the wave vector of an electron in the metal contact which lies along the z axis, and let $k_{\parallel}$ represent the magnitude of the wave vector of an electron in the metal contact parallel to the surface of the specimen; then

$$k_{lz} = k_l \cos\theta, \qquad (4)$$

$$k_{\parallel} = k_l \sin\theta. \qquad (5)$$

The z dependence of the wave function χ of an electron is described in a generalized CDMT formalism by

$$-\frac{\hbar^2}{2m_l}\frac{d^2}{dz^2}\chi=\frac{\hbar^2}{2m_l}k_{lz}^2\chi,\quad z\leqslant 0, \tag{6}$$

$$\left(-\frac{\hbar^2}{2m_r}\frac{d^2}{dz^2}+\frac{\hbar^2}{2m_\phi}k_\parallel^2+V(z)-\zeta_r+V_a\right)\chi=E\chi,\quad 0\leqslant z\leqslant d, \tag{7}$$

$$\left(-\frac{\hbar^2}{2m_r}\frac{d^2}{dz^2}+\frac{\hbar^2}{2m_\phi}k_\parallel^2-\zeta_r+V_a\right)\chi=E\chi,\quad z\geqslant d. \tag{8}$$

In Eqs. (7) and (8), ζ_r and V_a are, respectively, the Fermi energy in the semiconductor and potential energy associated with an applied bias. The mass m_ϕ is derived from Stratton and Padavoni's[5] analysis and characterizes the anisotropy of the ellipsoidal energy surfaces. One can write

$$m_\phi=2m_{\text{tr}}[1+\gamma+(1-\gamma)\cos(2\phi)]^{-1}, \tag{9}$$

where

$$\gamma=[\cos^2\Theta+m_{\text{long}}(\sin^2\Theta)/m_{\text{tr}}]^{-1}. \tag{10}$$

In Eqs. (7) and (8), d represents the distance from the metal contact to the point at which the barrier potential vanishes, i.e., $V(d)=0$.

Now, let

$$E'=E+\zeta_r-V_a \tag{11}$$

and

$$E_\perp\equiv\frac{\hbar^2k_{rz}^2}{2m_r}=E'-\frac{\hbar^2}{2m_\phi}k_l^2\sin^2\theta, \tag{12}$$

where k_l is fixed by E', using Eqs. (3) and (11). With these definitions, Eqs. (7) and (8) become

$$\left(-\frac{\hbar^2}{2m_r}\frac{d^2}{dz^2}+V(z)\right)\chi=E_\perp\chi, \tag{7a}$$

for $0\leqslant z\leqslant d$, and

$$-\frac{\hbar^2}{2m_r}\frac{d^2}{dz^2}\chi=\frac{\hbar^2}{2m_r}k_{rz}^2\chi, \tag{8a}$$

for $z\geqslant d$.

The transmission coefficient $T_{l\to r}$, is obtained from solving Eqs. (6), (7a), and (8a), requiring continuity of χ and its flux. Hence

$$\chi(-0)=\chi(+0),\quad \frac{1}{m_l}\frac{d\chi}{dz}\bigg|_{z=-0}=\frac{1}{m_r}\frac{d\chi}{dz}\bigg|_{z=+0}. \tag{13}$$

Furthermore, for $z\geqslant d$,

$$\chi=T_{l\to r}e^{ik_{rz}(z-d)}, \tag{14}$$

with k_{rz} being real, i.e., representing propagating solutions. This means that for a fixed value of E, E', or k_l in Eq. (12)

$$0\leqslant E_\perp\leqslant E'. \tag{15}$$

It is shown in Appendix A that

$$|T_{l\to r}|^2=K_{lz}^2D(E_\perp)/|K_{lz}-i\lambda w_1(E_\perp)|^2, \tag{16}$$

where K_{lz} and λ are defined by CDMT,

$$K_{lz}=\lambda\frac{m_r}{m_l}k_{lz},\quad \frac{1}{\lambda^4}=\frac{16\pi e^2n_rm_r}{\hbar^2\epsilon_r}. \tag{17}$$

For ellipsoidal energy surfaces,

$$k_{lz}=\left(\frac{2m_l}{\hbar^2}\right)^{1/2}\left[\frac{m_\phi}{m_l}E_\perp+\left(1-\frac{m_\phi}{m_l}\right)E'+\zeta_l-\zeta_r+V_a\right]^{1/2}. \tag{18}$$

The quantity $w_1(E_\perp)$ is the logarithmic derivative of $\chi(z)$ at the metal-semiconductor contact $z=0$. An inspection of Eq. (16) shows that the only dependence of $|T_{l\to r}|^2$ on E' or m_ϕ is through K_{lz}.

The current density for $T=0$ can be now written as

$$j=\frac{8e^3n_r}{\pi\hbar\epsilon_r}\left\langle\frac{m_\phi}{m_r}\int_{K_1}^{K_2}dK\,K\int_0^K dK_{rz}\,K_{rz}^2D(E_\perp)\times\frac{K_{lz}}{|K_{lz}-i\lambda w_1(E_\perp)|^2}\right\rangle, \tag{19}$$

where $\langle\ \rangle$ means an average over ϕ is to be taken. In deriving Eq. (19), we have introduced new variables K, K_{rz} replacing E' and $E_\perp$, where

$$K_{rz}=\lambda k_{rz},\quad E_\perp=\hbar^2K_{rz}^2/2\lambda^2m_r\ . \tag{20}$$

E' is related to K in the same way $E_\perp$ is related to K_{rz}. In Appendix B, it is shown that Eq. (19) can be reduced to

$$j=(8e^3n_r/\pi\hbar\epsilon_r)(m_l/m_r)^{1/2}(L_2-L_1), \tag{21}$$

where

$$L_j=\int_0^{K_j}dk\,K^2D(E_\perp)H_j(K), \tag{22}$$

with

$$K_j=\lambda[(2m_r/\hbar^2)E_j]^{1/2}, \tag{23}$$

$$E_\perp=\max[\zeta_r-V_a,\ 0],\quad E_2=\zeta_r. \tag{24}$$

In Eq. (22), $E_\perp$ is defined by Eq. (20), with K_{rz} replaced by K, and the functions $H_j(K)$ are given by

$$H_j(K)=\langle(m_\phi/m_r)(1-m_\phi/m_l)^{-1}[H(K_j;K)-H(K;K)]\rangle. \tag{25}$$

The function $H(K_1;K)$, with $K_1=K_j$ or K for brevity, is

$$H(K_1;K)=G(K_1;K)-\Gamma_{2I}\ln\{[G(K_1;K)]^2+\Gamma_{2R}^2\}+[1-(\Gamma_{2I}/\Gamma_{2R})^2]\Gamma'_{2R}\arctan[\Gamma_{2R}/G(K_1;K)], \tag{26}$$

where

$$G(K_1;K)=\Gamma_{2I}+\left[\Gamma_1^2+\frac{m_\phi}{m_l}K^2+\left(1-\frac{m_\phi}{m_l}\right)K_1^2\right]^{1/2}. \tag{27}$$

One should note that $G(K_1;K)$ is independent of K_1 when $m_\phi=m_l$, so that $H(K_1;K)=H(K;K)$, and no difficulty arises in Eq. (25) if this circumstance should arise. The quantities Γ_{2R} and Γ_{2I} are given by

$$\Gamma_{2R} = \eta\,|\mathrm{Re}(\lambda w_1)|,\quad \Gamma_{2I} = \eta\,\mathrm{Im}(\lambda w_1) > 0, \tag{28}$$

where the inequality is proved in Appendix A. Finally,

$$\Gamma_1 = \lambda[(2m_r/\hbar^2)(\zeta_l - \zeta_r + V_a)]^{1/2},\quad \eta = (m_l/m_r)^{1/2}. \tag{29}$$

A. CDMT approximation

From the CDMT paper, one finds that $w_1 \cong -d/2\lambda^2$, where

$$d = [(V_b + \zeta_r - V_a)\epsilon_r/2\pi e^2 n_r]^{1/2}. \tag{29}$$

By using $\Gamma(z)\Gamma(1-z) = \pi/\sin\pi z$, one finds an expression analytically equivalent to that derived by CDMT for D, i.e.,

$$D_{\mathrm{CDMT}} = (4/\pi)(\tfrac{1}{2}\zeta_0^2)^{2z} e^{(-\zeta_0^2/2)}/Q, \tag{30}$$

$$Q = \pi^{-2}[\cos^2\pi z\,\Gamma(\tfrac{1}{2}+z)^2 + \sin^2\pi z\,(z-\tfrac{1}{4})\Gamma(z)^2], \tag{31}$$

where

$$\zeta_0 = d/\lambda,\quad z = \tfrac{1}{4} + \tfrac{1}{2}K_{rz}^2. \tag{32}$$

(One should note that our procedure has eliminated Gamma functions of zero and negative arguments, which are computationally nasty.)

In general, w_1 is complex, but in the CDMT approximation it is real, as stated above. Hence, $|K_{lz} - i\lambda w_1|^2 = K_{lz}^2 + (\tfrac{1}{2}\zeta_0)^2$ in this approximation. Approximate and exact values of D and $g \equiv 1 + 2w_1\lambda^2/d$ are given in Table I.

TABLE I. Numerical comparison of the exact and approximate (CDMT) values of D and g functions in the transmission coefficient: $\zeta_l = 8600$ meV; $\zeta_r = 22.2$ meV; $n_D = 6.2\times10^{18}$ cm^{-3}; $m_r = 0.12\,m_0$; $V_b = 640$ meV (note that $g_{\mathrm{CDMT}} = 0$).

V_a (mV)	$E_\perp$ (meV)	D_{CDMT}	D_{exact}	Re(g)	Im(g)
−150	5	2.67×10^{-9}	2.62×10^{-9}	0.0245	5.14×10^{-11}
	25	6.77×10^{-9}	6.54×10^{-9}	0.0376	2.87×10^{-10}
	50	2.22×10^{-8}	2.09×10^{-8}	0.0541	1.30×10^{-9}
	75	7.41×10^{-8}	6.75×10^{-8}	0.0710	5.12×10^{-9}
	100	2.45×10^{-7}	2.15×10^{-7}	0.0882	1.88×10^{-8}
	125	7.85×10^{-7}	6.56×10^{-7}	0.1057	6.43×10^{-8}
	150	2.37×10^{-6}	1.88×10^{-6}	0.1237	2.02×10^{-7}
	175	6.75×10^{-6}	5.02×10^{-6}	0.1421	5.83×10^{-7}
	195	1.50×10^{-5}	1.06×10^{-5}	0.1571	1.29×10^{-6}
0	5	2.15×10^{-7}	2.09×10^{-7}	0.0303	4.55×10^{-9}
	25	5.12×10^{-7}	4.89×10^{-7}	0.0465	2.38×10^{-8}
	50	1.56×10^{-6}	1.44×10^{-6}	0.0672	9.90×10^{-8}
	75	4.80×10^{-6}	4.27×10^{-6}	0.0884	3.59×10^{-7}
	100	1.47×10^{-5}	1.25×10^{-5}	0.1102	1.21×10^{-6}
	125	4.37×10^{-5}	3.48×10^{-5}	0.1326	3.78×10^{-6}
	150	1.22×10^{-4}	9.10×10^{-5}	0.1558	1.08×10^{-5}
	175	3.22×10^{-4}	2.21×10^{-4}	0.1797	2.85×10^{-5}
	195	6.73×10^{-4}	4.31×10^{-4}	0.1994	5.85×10^{-5}
150	5	1.67×10^{-5}	1.62×10^{-5}	0.0398	3.40×10^{-7}
	25	3.70×10^{-5}	3.48×10^{-5}	0.0612	1.92×10^{-6}
	50	1.02×10^{-4}	9.20×10^{-5}	0.0889	7.19×10^{-6}
	75	2.86×10^{-4}	2.44×10^{-4}	0.1176	2.34×10^{-5}
	100	7.96×10^{-4}	6.36×10^{-4}	0.1476	7.02×10^{-5}
	125	2.14×10^{-3}	1.58×10^{-3}	0.1789	1.95×10^{-4}
	150	5.45×10^{-3}	3.64×10^{-3}	0.2120	4.93×10^{-4}
	175	1.30×10^{-2}	7.79×10^{-3}	0.2470	1.14×10^{-3}
	195	1.36×10^{-2}	1.56×10^{-2}	0.2767	2.10×10^{-3}

B. Approximate tunneling-current expressions for $\zeta_l - \zeta_r \gg |V_a|$

In this paper, we are primarily concerned with n-Ge Schottky barrier tunneling without impurity or phonon assistance. In this instance, our $w_1 \approx -d(2\lambda^2)$, i.e., CDMT with a negligible imaginary part. Furthermore, as long as the reverse-bias potential energy V_a is small compared to $\zeta_l - \zeta_r$, $\Gamma_1^2 \gg m_\phi K^2/m_l + (m_l - m_\phi)K_1^2/m_l$ in Eq. (27) and one can power series expand $G(K_1;K)$ in terms of $(1 - m_\phi/m_l)(K_1^2 - K^2)/(\Gamma_1^2 + K^2)$ in order to cancel out the $1 - m_\phi/m_l$ in the denominator of Eq. (25). Numerical investigations indicate that one need only go to second-order terms.

Preliminary investigations show that w_1 can vary rapidly with $E_\perp$ and V_a near a resonance in $D(E_\perp)$ associated with impurity-assisted tunneling. In this situation, Γ_{2R} can vanish or even become positive. However, it appears as if Γ_{2I} will still be small. Hence, in the remainder of this paper, we approximate $H(K_1;K)$ by

$$H(K_1;K) \cong G(K_1;K) + \Gamma_{2R}\arctan[\Gamma_{2R}/G(K_1;K)]. \tag{33}$$

Using the remarks made above, one finds that Eq. (25) reduces to

$$H_j(K) \cong \frac{\Gamma_{2R}}{2\sqrt{\gamma}}\left(\frac{m_{\mathrm{tr}}}{m_r}\right)\frac{G_0^3}{1+G_0^2} \times\left[\frac{E_j - E_\perp}{E_b + E_\perp} - \frac{1}{4}\left(\frac{G_0^2 - 1}{G_0^2 + 1}\right)\left(\frac{E_j - E_\perp}{E_b + E_\perp}\right)^2 \times\left(1 - \frac{m_{\mathrm{tr}}(1+\gamma)}{2m_l\gamma}\right)\right], \tag{34}$$

where

$$E_b = \zeta_l - \zeta_r + V_a, \tag{35}$$

$$G_0 = \lambda[2m_r(E_b + E_\perp)]^{1/2}/\hbar\Gamma_{2R}, \tag{36}$$

and

$$\Gamma_{2R} = (m_l/m_r)^{1/2}\lambda\,|\mathrm{Re}\,w_1(E_\perp)|. \tag{37}$$

At this point, one should note that the zeroth-order approximation to j [Eq. (19)] results from ignoring the dependence of K_{lz} upon K, K_{rz}, and m_ϕ, using

$$K_{lz} \cong \lambda(m_r/m_l)[2m_l(\zeta_l - \zeta_r + V_a)]^{1/2}/\hbar. \tag{38}$$

With this approximation, j is given by Eqs. (21) and (22) [or obtained directly by integrating Eq. (19) by parts with respect to K], using

$$H_j(K) \cong \left\langle\frac{m_\phi}{m_r}\right\rangle\frac{G_{00}^3}{1+G_{00}^2}\,\frac{E_j - E_\perp}{2E_b}\,\Gamma_{2R}, \tag{39}$$

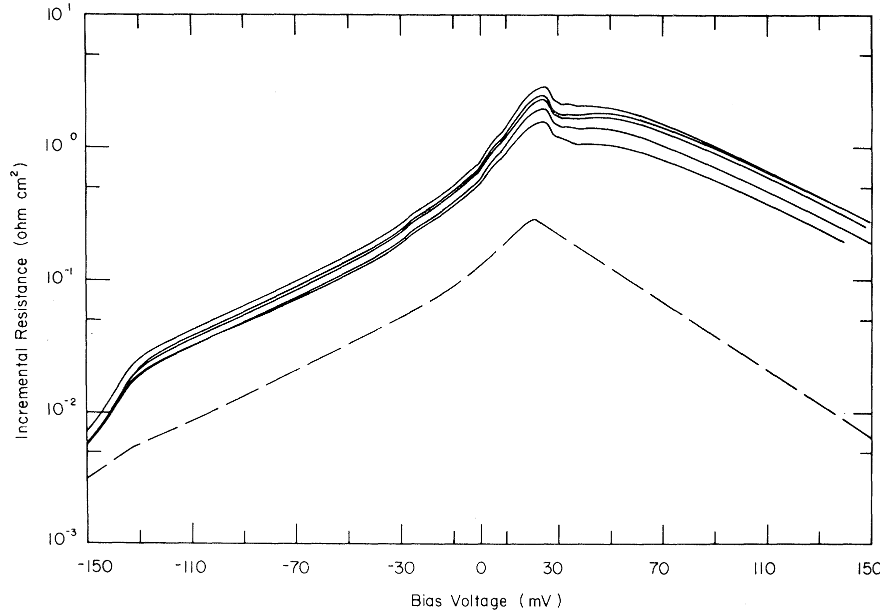

FIG. 1. Incremental resistance AdV/dI vs bias voltage. The dashed curve is the theoretical prediction for a doping density of 6.2×10^{18} cm^{-3} and barrier height of 0.640 eV. The solid curves are experimental results at 4.2 °K for samples with doping density of $6.2\pm0.3\times10^{18}$ cm^{-3} and barrier height of 0.64 $\pm$0.03 eV.

where G_{00} means G_0 with $E_\perp=0$. [This result is also a zeroth-order approximation to Eq. (33).]

This result shows the dependence of j upon the crystal orientation relative to the surface. Obviously, by comparison of Eqs. (33) and (34) (or by direct integration),

$$\langle m_\phi/m_r\rangle=(1/\sqrt{\gamma})(m_{tr}/m_r). \qquad (40)$$

For a [100] surface for Ge, $\cos^2\Theta=\frac{1}{3}$, $m_{long}/m_{tr}\cong20$, $m_r\cong0.12\ m_0$, $m_{tr}=0.082\ m_0$, $\gamma=\frac{3}{41}$, $\langle m_\phi/m_r\rangle\cong2.53$. This is the factor obtained by CDMT, presumably based on their numerical analysis.

IV. RESULTS AND DISCUSSION

The measured values of AdV/dI for five samples are displayed in Fig. 1. Barrier height and doping-density measurements were performed for all five of these samples. The barrier height, as described in the Sec. II, was determined to be 0.64 ± 0.03 eV. The doping density for these particular samples was $(6.2\pm0.3)\times10^{18}$ cm^{-3}. A theoretical curve for this barrier height and doping density is also presented in Fig. 1. For all the theoretical curves presented here, parameters appropriate to In–Ge junctions were used, namely, $m_t=m_0$, $\zeta_t=8.6$ eV, and $\epsilon_r=16\epsilon_0$. Also these theoretical curves include a factor of 4 to include tunneling to the four equivalent L_1 ellipsoids. Considering the large uncertainty in the parameters used in the theory, the agreement between theory and experiment is acceptable for tunneling to the four ellipsoids. The order-of-magnitude numerical agreement is all that can be expected. Without the abrupt steps in resistance caused by phonon-assisted tunneling (see Sec. V), the shape of the curves would be in very good agreement, except that the measured resistance change for high forward bias is not as great as the change predicted by theory. This shape disagreement was also found for antimony- and arsenic-doped junctions.[2] The effect of the upper-conduction-band minimum, which results in the dramatic decrease in resistance for negative bias around 130 mV, seems to be greatly underestimated by the theory. The upper-conduction-band minimum (Γ_2') in heavily doped germanium is reported[6] to be 0.154 eV above the lower-conduction-band minima (L_1). The Fermi level is these samples is approximately 22 meV, resulting in an onset of tunneling to the upper-conduction-band minimum around −132 mV.

For comparison to the CDMT theoretical results, it should be noted that in the theoretical results presented here, for most biases, the resistance is a factor of 2.5 lower owing to the correct treatment of the ellipsoidal energy surfaces and that for large negative bias the resistance is further reduced owing to the inclusion of tunneling to the upper-conduction-band minimum. Although for tunneling to the four ellipsoids the agreement between theory and experiment is better for CDMT than for the correct treatment given here, this is not meaningful because, owing to the uncertainty in the parameters used in the theory, both theories agree with the experiment.

At biases of approximately ±8, ±28, ±31, and ±36 mV steps in the resistance occur because of the onset of phonon-assisted tunneling. These effects are illustrated more clearly in Fig. 2, where, for one of the samples for which 4.2 °K data is presented in Fig. 1, $(1/A)dI/dV$ and $(1/A)d^2I/dV^2$ for data taken at 1.35 °K are presented. A comparison to theory for this effect will be given in Sec. V.

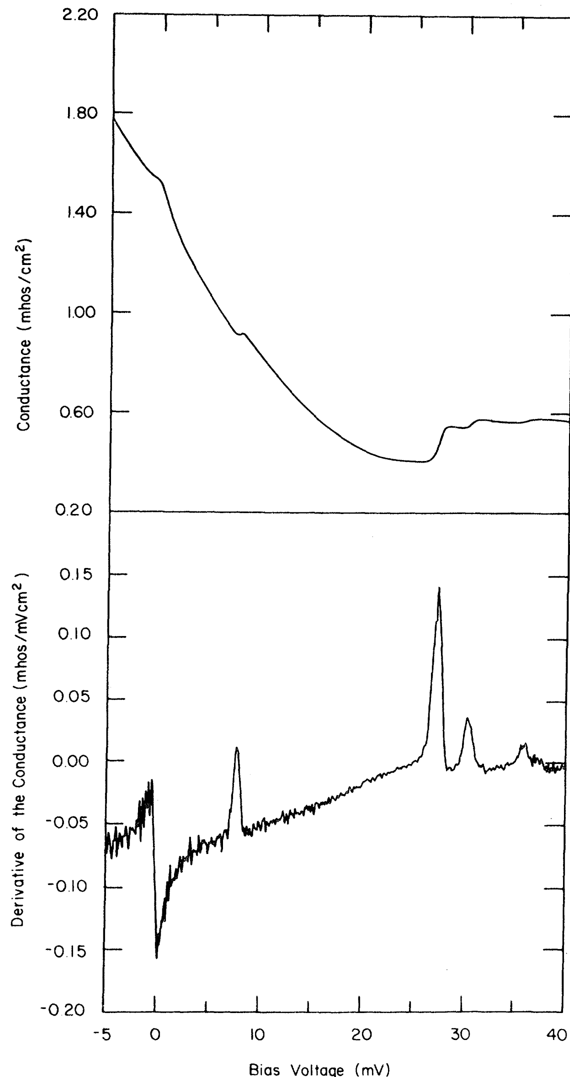

FIG. 2. Conductance and derivative of the conductance taken from experimental data at 1.35 °K for one of the samples presented in Fig. 1. (a) Conductance $[(1/A)dI/dV]$ vs bias voltage. (b) Derivative of the conductance $[(1/A)d^2I/dV^2]$ vs bias voltage.

Here it is important to point out that the phonon-assisted tunneling is large and makes difficult a precise determination of the peak of the non-phonon-assisted-tunneling curve. This is significant because, as shown in Fig. 1, the calculated resistance peaks at a bias equal to the Fermi degeneracy. (The density of states effective mass m_d^* for each of the four ellipsoids is $0.22m_0$ and the Fermi degeneracy is given by $\zeta_r = (\hbar^2/2m_d^*)[(\frac{3}{4})\pi^2 n_D]^{2/3}$. For $n_D = 6.2 \times 10^{18}$ cm^{-3}, $\zeta_r = 22.2$ meV.) There appears to be a peak in the experimental curves for biases just below the 28-mV phonon-resistance steps, but the phonon steps rule out a definite conclusion. Using the minimum of the curve in Fig. 2(a) and the zero of the curve in Fig. 2(b) a value of approximately 24 meV is obtained. In any event, the curves, although apparently peaking in the right area, do not peak precisely at the theoretically predicted value of 22.2 mV. Similar variations from precise agreement have been reported[13] for other metal–Ge (n type) and metal–Si (n type) junctions. One could also argue that for the curves in Fig. 1 after subtraction of phonon-conductance steps there is a peak at higher biases (~ 50 mV). This peak which could possibly be due to the bias dependence of the phonon-assisted tunneling is not due to a Fermi degeneracy of 50 meV. This latter conclusion is drawn from the fact that the onset of tunneling of the Γ_2' conduction band occurs at a bias of approximately 130 mV, corresponding to a Fermi level of approximately 20–25 meV. If the Fermi degeneracy were 50 meV the onset of tunneling to the Γ_2' conduction band would occur at a bias of approximately 100 mV. Shown in Fig. 3 are the results for a higher doped sample, for which the phonon peaks are less significant. (For this sample the doping density and area were measured but the barrier height was not. For the theoretical calculation the 0.64-eV barrier height found for all measured samples was used.) The Fermi degeneracy for this sample is 32.1 meV, corresponding to the point at which the theoretical curve peaks. In the experimental curve the phonon steps are still a problem, but with the steps removed the curve apparently would peak in the right area.

Finally, it should be reluctantly noted that owing to the large uncertainty in the values of the parameters used in the one-electron theory it is impossible to draw any definite conclusions about the dependence of the tunnel current on dopant type. Junctions doped with antimony,[2] arsenic,[2] or phosphorus agree within experimental error with the one-electron theory. Combescot and Schreder[4] have made calculations of impurity-assisted tunneling in metal–Ge (n) junctions and estimate that it would be greatest in arsenic-doped junctions and its conductance would have a magnitude of approximately 40% of the one-electron tunneling conductance. Based on their arguments, phosphorus-doped junctions would be expected to have smaller but same-order-of-magnitude impurity-assisted tunneling. Antimony-doped junctions would have a very small impurity-assisted contribution. The experiment reported here and the work on antimony and arsenic[2] have order-of-magnitude uncertainties and agree within this uncertainty with the one-electron theory, thereby precluding drawing definite conclusions about impurity-assisted effects of the order of magnitude estimated by Combescot and Schreder.[4]

V. PHONON-ASSISTED TUNNELING

For one of the samples for which 4.2 °K data is presented in Fig. 1, $(1/A)dI/dV$ and $(1/A)d^2I/dV^2$ for

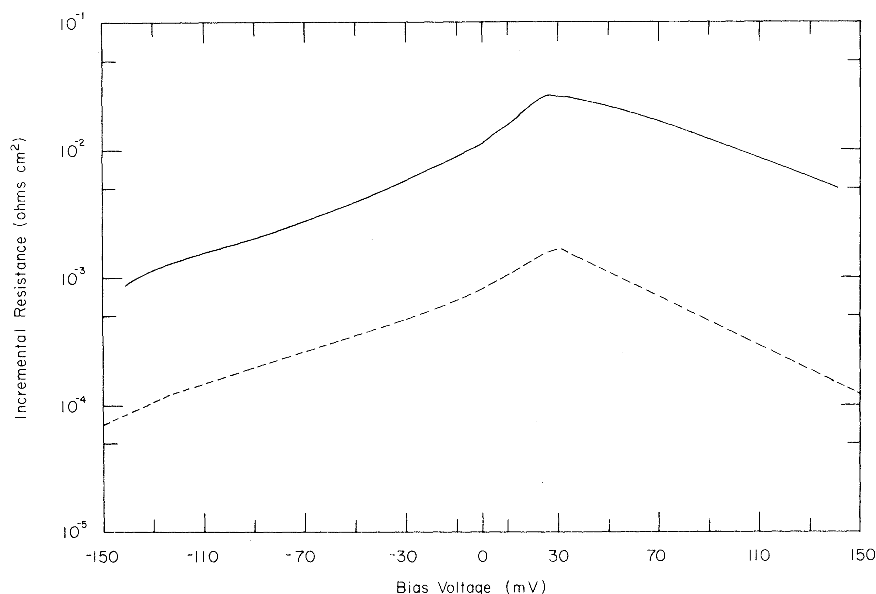

FIG. 3. Incremental resistance AdV/dI vs bias voltage. The dashed curve is the theoretical prediction for a doping density of 1.08×10^{19} cm^{-3} and barrier height of 0.640 eV. The solid curve is the experimental results at 4.2 °K for a sample with a measured doping density of 1.08 ± 0.05 $\times10^{19}$ cm^{-3}.

data taken at 1.35 °K are presented in Fig. 2. A magnetic field of magnitude 4.30 kG was applied. The zero-bias anomaly (conductance peak) frequently seen in tunnel junctions is readily observable. The step increases in conductance associated with phonon-assisted tunneling are also clearly illustrated here at the bias voltages corresponding to the four zone-boundary phonon energies (TA ~ 8 mV, LA ~ 28 mV, LO ~ 31 mV, TO ~ 36 mV). This is the first observation of strong phonon-assisted tunneling in metal–Ge:P junctions, although data of similar strength have been reported[14] for phosphorus-doped p–n junctions. For doping to approximately 6×10^{18} cm^{-3}, such as illustrated in Fig. 2, the LA conductance step is approximately 0.12 Ω^{-1}cm^{-2}. This agrees very well with the 0.1-Ω^{-1}cm^{-2} value predicted by Davis and Steinrisser.[15] The ordering of the four phonon types in decreasing conductance-step magnitude is LA, TA, LO, and TO. This ordering is the same as that observed in arsenic- and antimony-doped metal–semiconductor junctions[2] and all three dopant types in p–n junctions.[14] The magnitude of the conductance steps for the TA, LO, and TO phonons are 0.05, 0.04, and 0.02 Ω^{-1}cm^{-2}, respectively, which are similar to those reported for antimony- and arsenic-doped metal–semiconductor junctions and, except for the TO phonon, are in reasonable agreement with theoretical predictions.[2] The four phonon energies determined from the peaks of $(1/A)d^2I/dV^2$ agree within experimental error (0.2 mV) with those reported by Payne[16] for p–n junctions.

In p–n junctions the strength of the phonon peaks compared to the background conductance varies greatly with dopant type.[14] Combescot and Schreder[7] have found for all three dopant types qualitative agreement between experiment and their theoretical prediction of the ratio of the LA phonon step to a background conductance (at $V=0$), which is entirely impurity-assisted tunneling. As these authors discussed, the three dopant types give significantly different impurity-assisted tunneling,[4] making the large variation in the ratio for different dopants reasonable. These authors also discussed metal-semiconductor junctions and, specifically, metal–germanium junctions. They point out that the calculated ratio of the LA conductance step to background conductance (at $V=0$) which is entirely specular tunneling gives reasonable agreement with experiment on antimony- and arsenic-doped junctions. Although they do not make predictions specifically for phosphorus-doped junctions, a comparison of our results to their predictions is reasonable, as little or no impurity-type dependence is exhibited. For a doping density of $(6.2\pm0.3)\times10^{18}$ cm^{-3} our value of their ratio is 0.1, which is in good agreement with their calculated value of 0.14 for $n_D=6.7\times10^{18}$ cm.$^{-3}$

ACKNOWLEDGMENTS

The authors would like to thank Miss L. Roth of Purdue University for the crystal used in these experiments. They would also like to thank the personnel of the electronics and machine shops of the University of Kentucky for their assistance in designing and building the equipment used. Finally, they would like to thank James T. Wimmers for his assistance.

APPENDIX A: NUMERICAL PROCEDURE FOR DETERMINING $|T_{l\to r}|^2$

A simple numerical procedure for determining $|T_{l\to r}|^2$ is given in this appendix. Equation (16) of

the text is also established.

Equations (6), (7a), (8a), and (14), together with the boundary conditions, fix $T_{l\to r}$. $\chi(z)$ satisfies

$$\chi(z)=e^{ik_{lz}z}+Re^{-ik_{lz}z},\quad z\leq 0. \tag{A1}$$

In the barrier region, we take

$$\chi_{j-1}(z)=A_{j-1}\cosh\kappa_j(z-z_{j-1}) + B_{j-1}[\sinh\kappa_j(z-z_{j-1})]/\kappa_j \tag{A2}$$

for the region

$$z_{j-1}\leq z\leq z_j,$$

with

$$\kappa_j^2\equiv\frac{1}{z_j-z_{j-1}}\int_{z_{j-1}}^{z_j}dz\,\frac{2m_r}{\hbar^2}\,[V(z)-E_\perp]\,. \tag{A3}$$

In the limit $z_j-z_{j-1}\to 0$, our procedure will give the exact $\chi(z)$; in practice, we get very good numerical accuracy by taking no more than 50 intervals for the n-Ge Schottky-barrier potentials used in this paper.

At $z=z_N\equiv d$, Eq. (14) gives

$$T=A_{N-1}C_N+B_{N-1}S_N/\kappa_N, \tag{A4}$$

which can be written

$$T=A_1\frac{A_2}{A_1}\frac{A_3}{A_2}\cdots\frac{A_{N-1}}{A_{N-2}}\,(C_N+S_Nw_{N-1}/\kappa_N), \tag{A5}$$

where C_j and S_j denote cosh and sinh functions whose arguments are $\kappa_j[z_j-z_{j-1}]$, and

$$w_j\equiv B_j/A_j. \tag{A6}$$

From the boundary conditions (13), we get

$$\begin{aligned}C_jB_{j-1}+S_j\kappa_jA_{j-1}&=B_j\,,\\ B_{j-1}S_j/\kappa_j+C_jA_{j-1}&=A_j\,.\end{aligned} \tag{A7}$$

From the second equation of (A7), one obtains

$$A_j/A_{j-1}=C_j+w_{j-1}S_j/\kappa_j\,, \tag{A8}$$

so that (A5) yields

$$T=A_1\prod_{j=2}^{N}\left(C_j+\frac{S_jw_{j-1}}{\kappa_j}\right)\,. \tag{A9}$$

To obtain w_{j-1} from w_j, solve (A7) for B_{j-1} and A_{j-1} in terms of B_j and A_j, then take the ratio B_{j-1}/A_{j-1}, which gives, using (A6),

$$w_{j-1}=\frac{C_jw_j-\kappa_jS_j}{C_j-S_jw_j/\kappa_j}\,, \tag{A10}$$

where $j=2,\ 3,\ \ldots N$. Matching derivatives of χ at $z=z_N$ gives

$$ik_{rz}T=S_N\kappa_NA_{N-1}+C_NB_{N-1}\,, \tag{A11}$$

and taking the ratio of this equation to (A4), one gets the logarithmic derivative of $\chi(z)$ at $z_N=d$

$$w_N\equiv ik_{rz}=\frac{C_Nw_{N-1}+\kappa_NS_N}{C_N+S_Nw_{N-1}/\kappa_N}\,. \tag{A12}$$

Solving for w_{N-1} gives precisely the same equation as indicated by Eq. (A10), with $w_N=ik_{rz}$; hence $w_{N-1},\ w_{N-2},\ \ldots\ w_1$ are fixed sequently by (A10).

Since Im $(w_N)>0$, it is easy to show that Im $(w_j)>0$ for $j=2,\ 3,\ \ldots N$ using (A10). Furthermore, C_j, S_j/κ_j, and κ_jS_j are *real*, so that the denominator of (A10) can not vanish.

Finally, one has, using the boundary conditions at $z=z_1=0$,

$$1+R=A_1,\quad ik_{lz}(1-R)/m_l=B_1/m_r\,, \tag{A13}$$

so that

$$A_1=\frac{2m_rk_{lz}/m_l}{m_rk_{lz}/m_l-iw_1}\,. \tag{A14}$$

This establishes $T_{l\to r}=T$, using Eq. (A9), and one can write

$$|T_{l\to r}|^2=(K_{lz}^2/|K_{lz}-i\lambda w_1(E_\perp)|^2)\,D(E_\perp), \tag{A15}$$

where Eq. (17) relates K_{lz} to k_{lz}, $E_\perp$ is given by Eq. (12) in terms of k_{rz}, and

$$D(E_\perp)=4\prod_{j=2}^{N}\left|C_j+\frac{S_jw_{j-1}}{\kappa_j}\right|^2 \tag{A16}$$

depends upon $E_\perp$ only through the $\kappa_j(E_\perp)$ and k_{rz}. This establishes Eq. (16) as well as a simple and rapid procedure for calculating $|T_{l\to r}|^2$ for *any* potential-energy function which can be approximated by piecewise continuous segments, e.g., square-well impurity potentials as well as the Schottky-barrier potential.

Numerical comparisons of $D(E_\perp)$ using (A16) for the Schottky-barrier potential are presented in the text.

APPENDIX B: SIMPLIFICATION OF j FOR ARBITRARY POTENTIAL

In Appendix A, we proved that

$$|T_{l\to r}|^2=K_{lz}^2\,|K_{lz}-i\lambda\,w_1(E_\perp)|^{-2}D\,(E_\perp), \tag{B1}$$

where K_{lz} is given by Eqs. (17) and (18).

Owing to this special form of $|T_{l\to r}|^2$, it is always possible to collapse the double integration appearing in Eq. (19) for j to a single quadrature involving relatively simple analytic functions.

To do this, we note that the dependence of $|T_{l\to r}|^2/K_{lz}$ upon K and m_ϕ is through the factor $K_{lz}|K_{lz}-i\lambda\,w_1(E_\perp)|^{-2}$, which can be written

$$\chi=K_{lz}|K_{lz}-i\lambda\,w_1|^{-2}=K_{lz}[(K_{lz}+\lambda\,w_{1I})^2+(\lambda\,w_{1R})^2]^{-1}, \tag{B2}$$

where R and I refer to real and imaginary parts of w_1. This equation can be rewritten

$$\chi = \mathrm{Im}\{K_{lz}[K_{lz} - i\lambda(|w_{1R}| + iw_{1I})]^{-1}/\lambda|w_{1R}|\}. \quad \text{(B3)}$$

Now let

$$\Gamma_2 = (m_l/m_r)^{1/2}\lambda(|w_{1R}| + iw_{1I}) , \quad \text{(B4)}$$

and

$$G_0(K;K_{rz}) = [\Gamma_1^2 + (m_\phi/m_l)K_{rz}^2 + (1 - m_\phi/m_l)K^2]^{1/2} , \quad \text{(B5)}$$

then one can write

$$\chi = \left(\frac{m_r}{m_l}\right)^{1/2} \left\{G_0^{-1} - \Gamma_{2R}^{-1}\,\mathrm{Im}\left[\frac{\Gamma_2^2}{G_0^2 + \Gamma_2^2}\left(1 + i\frac{\Gamma_2}{G_0}\right)\right]\right\} , \quad \text{(B6)}$$

where Γ_1 is defined by Eq. (29). In Eq. (B6), $\Gamma_{2R} = \mathrm{Re}(\Gamma_2)$. Our idea is to use integral representations for χ so as to factor it into a sum of products of functions of K only and K_{rz} only.

For example,

$$G_0^{-1} = \pi^{-1/2}\int_{-\infty}^{\infty} dt\, e^{-t^2(\Gamma_1^2 + \alpha K^2 + \beta K_{rz}^2)}, \quad \text{(B7)}$$

where

$$\alpha = 1 - m_\phi/m_l, \quad \beta = m_\phi/m_l. \quad \text{(B8)}$$

We need to recall that Γ_2 is a function of K_{rz} only. To evaluate j using Eqs. (19) and (B6), we have a terms involving

$$F_{a;j} = \int_0^{K_j} dK\, K \int_0^K dK_{rz}\, F_a(K_{rz})[G_0(K;K_{rz})]^{-1}, \quad \text{(B9)}$$

which can be written

$$F_{a;j} = \pi^{-1/2}\int_{-\infty}^{\infty} dt\, e^{-t^2\Gamma_1^2}\int_0^{K_j} dK\, K e^{-t^2K^2\alpha} \times \int_0^K dK_{rz}\, F_a(K_{rz}) e^{-t^2\beta K_{rz}^2} .$$

Next, integrate by parts with respect to K, then

$$F_{a;j} = \int_0^{K_j} dK\, F_a(K)\pi^{-1/2}\int_{-\infty}^{\infty} dt\, e^{-t^2\Gamma_1^2} \times \frac{e^{-t^2(\alpha+\beta)K^2} - e^{-t^2(\alpha K_j^2 + \beta K^2)}}{2\alpha t^2}$$

$$= \int_0^{K_j} dK\, F_a(K)\,\frac{G_0(K_j;K) - G_0(K;K)}{\alpha} , \quad \text{(B10)}$$

where G_0 is defined by Eq. (B5).

The term in Eq. (B6) involving $(\Gamma_2^2 + G_0^2)^{-1}$ is handled by using

$$(X+Y)^{-1} = 2\int_0^\infty du\, u e^{-u^2(X+Y)}. \quad \text{(B11)}$$

The subsequent integrations can be carried out, and they yield

$$F_{b;j} = \int_0^{K_j} dK\, K\int_0^K dK_{rz}\, F_b(K_{rz})[\Gamma_2^2 + G_0(K;K_{rz})^2]^{-1}$$

$$= \int_0^{K_j} dK\, F_b(K)\frac{1}{2\alpha}\,\ln\left(\frac{\Gamma_1^2 + \Gamma_2^2 + \alpha K_j^2 + \beta K^2}{\Gamma_1^2 + \Gamma_2^2 + \alpha K^2 + \beta K^2}\right), \quad \text{(B12)}$$

where the argument of ln lies in the first quadrant of the complex plane.

To evaluate the remaining term in χ, one must use both Eqs. (B7) and (B11). One finds that

$$F_{c;j} = i\int_0^{K_j} dK\, K\int_0^K dK_{rz}\, F_c(K_{rz})(\Gamma_2^2 + G_0^2)^{-1}\Gamma_2 G_0^{-1} \quad \text{(B13)}$$

$$= -\int_0^{K_j} dK\, F_c(K)\left(\alpha^{-1}\ln\left[\frac{G_0(K;K) - i\Gamma_2}{G_0(K_j;K) - i\Gamma_2}\right] + \frac{1}{2\alpha}\,\ln\left[\frac{\Gamma_2^2 + G_0(K_j;K)^2}{\Gamma_2^2 + G_0(K;K)^2}\right]\right). \quad \text{(B14)}$$

The second term in (B14) cancels out the term denoted by (B12).

Using these results, we obtain the expression for j given by Eq. (21) of the text.

---

*Work supported in part by the National Science Foundation.

[1]F. Steinrisser, L. C. Davis, and C. B. Duke, Phys. Rev. 176, 912 (1968).

[2]L. C. Davis and F. Steinrisser, Phys. Rev. B 1, 614 (1970).

[3]J. W. Conley, C. B. Duke, G. D. Mahan, and J. J. Tiemann, Phys. Rev. 150, 466 (1966).

[4]R. Combescot and G. Schreder, J. Phys. C 6, 1363 (1973).

[5]R. Stratton and F. A. Padovani, Phys. Rev. 175, 1072 (1968).

[6]J. W. Conley and J. J. Tiemann, J. Appl. Phys. 38, 2880 (1967).

[7]R. Combescot and G. Schreder, J. Phys. C 7, 1318 (1974).

[8]E. L. Wolf and W. C. Compton, Rev. Sci. Instrum. 40, 1497 (1969).

[9]D. E. Cullen, E. L. Wolf, and W. D. Compton, Phys. Rev. B 2, 3157 (1970).

[10]J. G. Adler and J. E. Jackson, Rev. Sci. Instrum. 37, 1049 (1966).

[11]S. M. Sze and J. C. Irvin, Solid-State Electron. 11, 599 (1968); W. G. Spitzer, F. A. Trumbore, and R. A. Logan, J. Appl. Phys. 32, 1822 (1961).

[12]D. R. Fredkin and G. H. Wannier, Phys. Rev. 128, 2054 (1962).

[13]T. F. Tao and Yukun Hsia, Appl. Phys. Lett. 9, 291

(1968).
[14]R. N. Hall, *International Conference on Semiconductor Physics*, *Prague*, 1960 (Academic, New York, 1961), p. 193.
[15]The results of Davis and Steinrisser (Ref. 2) are plotted as a function of Fermi level or impurity concentration in G. Forest and E. Erlbach, Solid State Commun. 10, 1137 (1972).
[16]R. T. Payne, Phys. Rev. 139, A570 (1965).